Supporting Information for

Probing the Critical Dipole Moment to Support Excited Dipole-Bound States in Valence-Bound Anions

Chen-Hui Qian, Guo-Zhu Zhu, and Lai-Sheng Wang*

Department of Chemistry, Brown University, Providence, Rhode Island 02912, USA

Corresponding Author: *Lai-Sheng_Wang@brown.edu

Methods

Experimental methods. The experiment was carried out on our third-generation electrospray ionization photoelectron spectroscopy (ESI-PES) apparatus equipped with a high resolution photoelectron imaging system.[1] The halogen-substituted phenoxide anions (*p*-$XC_6H_4O^-$, X = F, Cl, Br, I) were produced by dissolving the corresponding phenols (4-fluophenol, 4-chlorophenol, 4-bromophenol, and 4-iodophenol from Aldrich-Sigma Inc.) in the MeOH/H_2O (9/1 volume ratio) mixed solvent adjusted to pH ~ 10 using NaOH. Anions from the ESI source were guided into the cryogenically cooled Paul trap[2] operated at 4.6 K and cooled by 1 mTorr He/H_2 buffer gas (4/1 volume ratio) in the trap for 0.1s. The anions were extracted from the ion trap at a 10 Hz repetition rate into a time of flight mass spectrometer. A mass gate was used to isolate the desired anions before crossing with a dye laser operated at 20 Hz in the interaction zone of the imaging lens. Photoelectrons were then extracted and focused onto a set of micro-channel plates coupled to a phosphor screen with a CCD camera.[3] Inverse-Abel transformation was used to reconstruct the images from the raw data using both the BASEX and pBASEX programs.[4,5]

Theoretical methods. The harmonic frequencies and dipole moments of the halogen substituted neutral radicals were calculated at the B3LYP/6-311++G(d,p) level using the Gaussian 09 package.[6]

REFERENCES

(1) Wang, L. S. Perspective: Electrospray Photoelectron Spectroscopy: From Multiply-Charged Anions to Ultracold Anions. *J. Chem. Phys.* **2015**, *143*, 040901.

(2) Wang, X. B.; Wang, L. S. Development of a Low-Temperature Photoelectron Spectroscopy Instrument Using an Electrospray Ion Source and a Cryogenically Controlled Ion Trap. *Rev. Sci. Instrum*. **2008**, *79*, 073108.

(3) León, I.; Yang, Z.; Liu, H. T.; Wang, L. S. The Design and Construction of a High-Resolution Velocity-Map Imaging Apparatus for Photoelectron Spectroscopy Studies of Size-Selected Clusters. *Rev. Sci. Instrum.* **2014**, *85*, 083106.

(4) Dribinski, V.; Ossadtchi, A.; Mandelshtam, V. A.; Reisler, H. Reconstruction of Abel-Transformable Images: The Gaussian Basis-Set Expansion Abel Transform Method. *Rev. Sci. Instrum*. **2002**, *73*, 2634−2642.

(5) Garcia, G. A.; Nahon, L.; Powis, I. Two-Dimensional Charged Particle Image Inversion Using a Polar Basis Function Expansion. *Rev. Sci. Instrum*. **2004**, *75*, 4989−4996.

(6) Frisch, M. J.; Trucks, G. W.; Schlegel, H. B.; Scuseria, G. E.; Robb, M. A.; Cheeseman, J. R.; Scalmani, G.; Barone, V.; Petersson, G. A.; Nakatsuji, H.; Li, X.; Caricato, M.; Marenich, A. V.; Bloino, J.; Janesko, B. G.; Gomperts, R.; Mennucci, B.; Hratchian, H. P.; Ortiz, J. V.; Izmaylov, A. F.; Sonnenberg, J. L.; Williams-Young, D.; Ding, F.; Lipparini, F.; Egidi, F.; Goings, J.; Peng, B.; Petrone, A.; Henderson, T.; Ranasinghe, D.; Zakrzewski, V. G.; Gao, J.; Rega, N.; Zheng, G.; Liang, W.; Hada, M.; Ehara, M.; Toyota, K.; Fukuda, R.; Hasegawa, J.; Ishida, M.; Nakajima, T.; Honda, Y.; Kitao, O.; Nakai, H.; Vreven, T.; Throssell, K.; Montgomery, J. A., Jr.; Peralta, J. E.; Ogliaro, F.; Bearpark, M. J.; Heyd, J. J.; Brothers, E. N.; Kudin, K. N.; Staroverov, V. N.; Keith, T. A.; Kobayashi, R.; Normand, J.; Raghavachari, K.; Rendell, A. P.; Burant, J. C.; Iyengar, S. S.; Tomasi, J.; Cossi, M.; Millam, J. M.; Klene, M.; Adamo, C.; Cammi, R.; Ochterski, J. W.; Martin, R. L.; Morokuma, K.; Farkas, O.; Foresman, J. B.; Fox, D. J. Gaussian 09, Revision C.01, Gaussian, Inc., Wallingford CT, 2009.

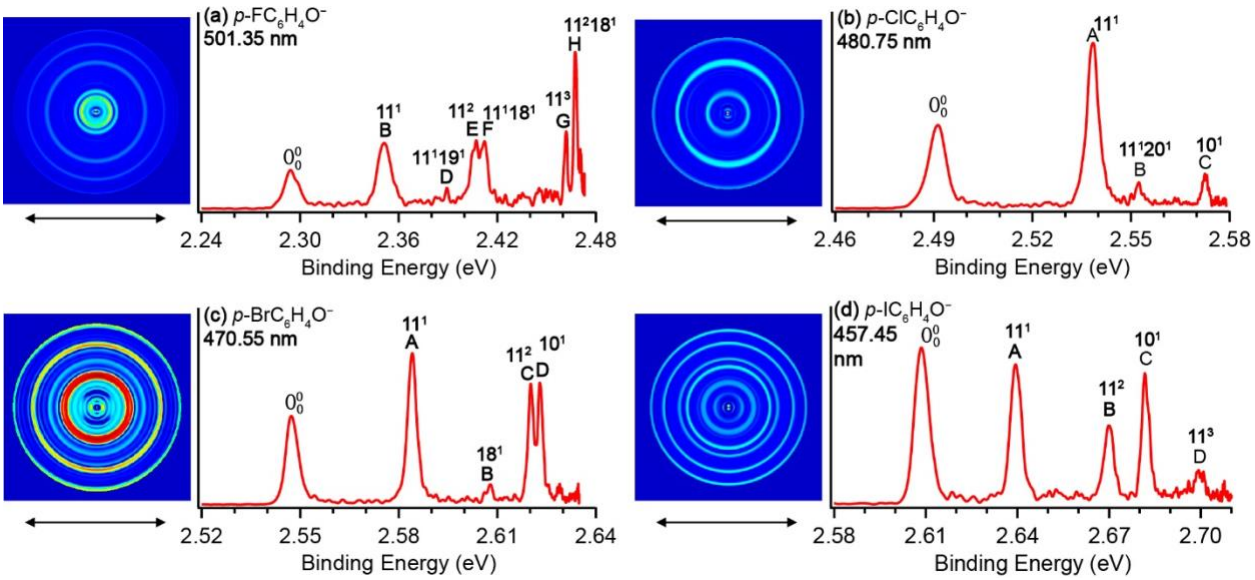

Figure S1. The photoelectron images and spectra of *p*-$XC_6H_4O^-$ (X = F, Cl, Br, I). The detachment wavelengths and the assignments of the observed vibrational features are given. The binding energies of the observed peaks are given in Tables S4 to S7, respectively. The double arrows below the images indicate the directions of the laser polarization.

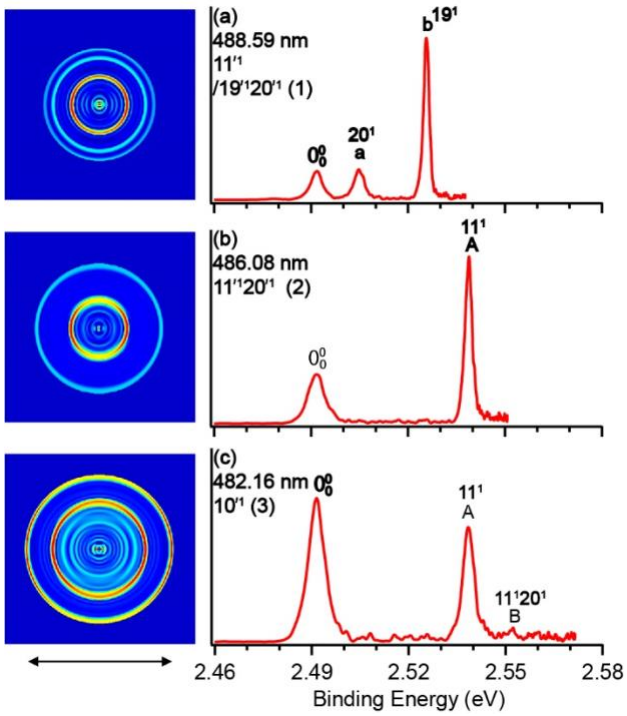

Figure S2. The resonant photoelectron images and spectra of *p*-$ClC_6H_4O^-$ at three wavelengths corresponding to the three DBS resonances in Figure 1b. The resonantly enhanced peaks are labeled in **bold** face. Peak 1 in Figure 1b is due to the $11'_1$ DBS level, but the appearance of strong peaks *a* (20_1) and *b* (19_1) in (a) suggest that there is a nearby overlapping combinational DBS vibrational level of $19'_120'_1$. The enhancement of peak A (11_1) in (b) and peak 0_{00} in (c) is due to autodetachment from DBS vibrational levels of $11'_120'_1$ and $10'_1$, respectively. The binding energies and frequencies of the observed vibrational peaks are given in Table S5. The double arrow below the images indicates the directions of the laser polarization.

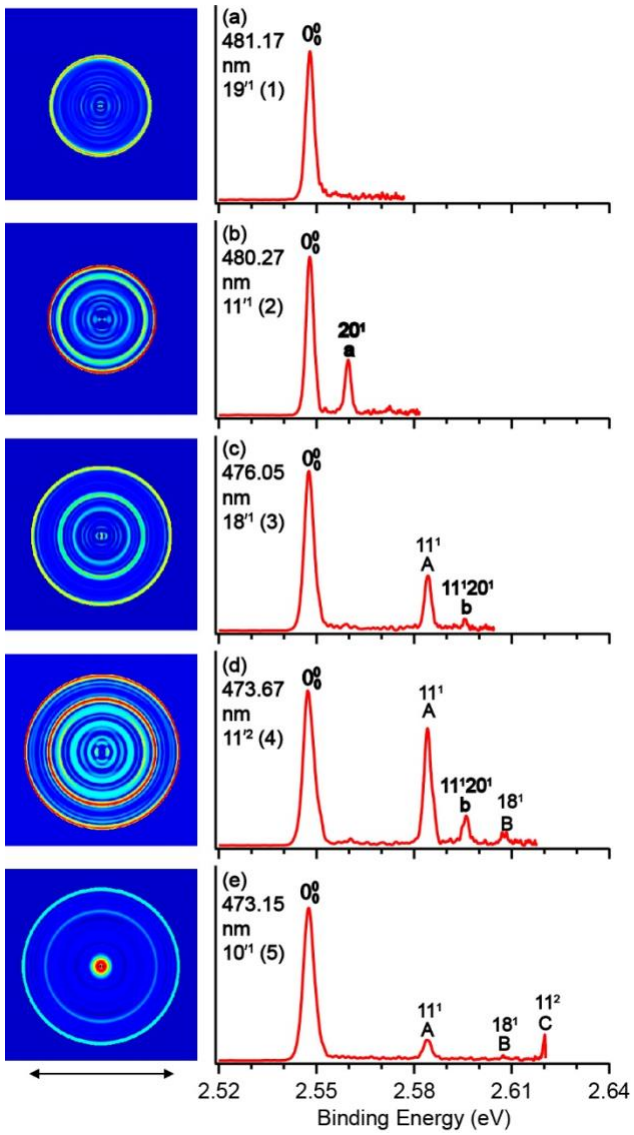

Figure S3. The resonant photoelectron images and spectra of *p*-$BrC_6H_4O^-$ at five wavelengths corresponding to the five DBS resonances in Figure 1c. The resonantly enhanced peaks are labeled in **bold** face. The enhancement of peak 0_{00} in (a) – (c) and (e) is due to autodetachment from the fundamental DBS vibrational levels of $19'_1$, $11'_1$, $18'_1$ and $10'_1$, respectively. In (d), peak 0_0 is enhanced and the $\Delta v = -2$ autodetachment is observed probably due to the anharmonic effect. The double arrow below the image indicates the directions of the laser polarization. The binding energies and frequencies of the observed vibrational peaks are given in Table S6.

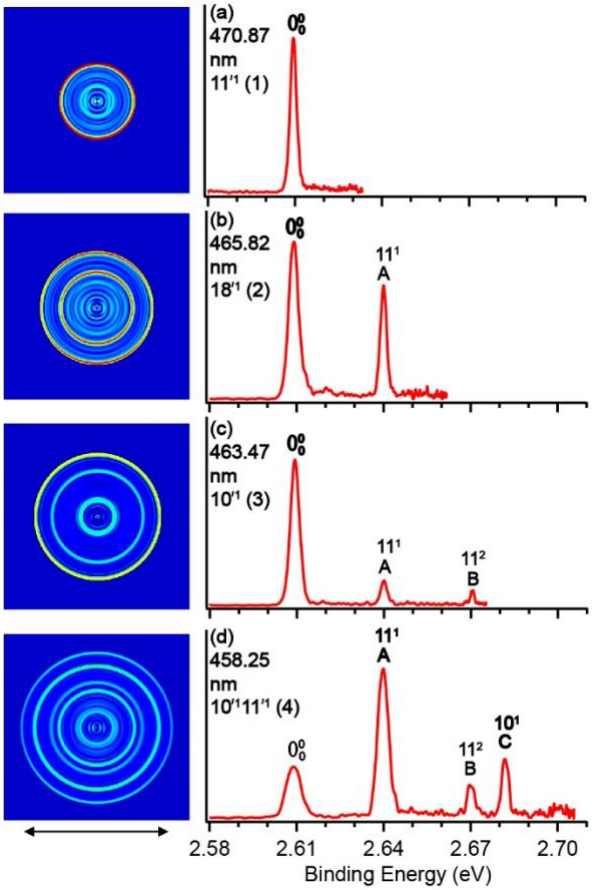

Figure S4. The resonant photoelectron images and spectra of *p*-$IC_6H_4O^-$ at the four wavelengths corresponding to the four DBS resonances in Figure 1d. The enhanced peaks are labeled in **bold** face. The enhancement of peak 0_{00} in (a) – (c) are due to $\Delta v = -1$ autodetachment from the fundamental DBS vibrational levels of $11'_1$, $18'_1$ and $10'_1$ of *p*-$IC_6H_4O^-$, while peak A (11_1) and peak C (10_1) in (d) are enhanced due to autodetachment from the combinational DBS vibrational level $10'_111'_1$. The double arrow below images indicates the directions of the laser polarization. The binding energies and frequencies of the observed vibrational peaks are given in Table S7.

Table S1. The calculated quadrupole moments and polarizabilities of *p*-XC_6H_4O (X = F to I and H) at the B3LYP/6-311++G(d,p) level of theory. The cross terms for the orientation of xy, xz, yz are all 0. In this case, only the terms in xx, yy, zz directions matter. The traceless quadrupole terms are represented by Q_{xx}, Q_{yy}, Q_{zz} in units of Debye.Å. The polarizabilities are represented by α_{xx}, α_{yy}, α_{zz} in units of $Bohr^3$. The isotropic polarizability is from averaging the polarizability in all three directions.

	Q_{xx}	Q_{yy}	Q_{zz}	α_{xx}	α_{yy}	α_{zz}	α (isotropic)
p-FC_6H_4O	1.2076	10.4277	-11.6352	39.590	76.062	103.222	72.96
p-ClC_6H_4O	1.1845	10.3122	-11.4967	45.856	81.856	138.135	88.62
p-BrC_6H_4O	2.0060	11.1116	-13.1176	50.907	86.052	156.234	97.73
p-IC_6H_4O	2.5031	10.9027	-13.4058	57.446	93.958	183.221	111.54
C_6H_5O	-1.9059	-4.5071	-6.4130	40.441	99.461	77.203	72.37

Table S2. The moments of inertia along the principle axes for *p*-XC_6H_4O (X = F to I and H). All the eigenvalues are shown in atomic unit. The calculation was done at the B3LYP/6-311++G(d,p) level of theory.

	X	Y	Z
p-FC_6H_4O	1507.87001	1179.15626	328.71374
p-ClC_6H_4O	2108.94119	1780.77959	328.16160
p-BrC_6H_4O	3074.90627	2746.58812	328.31815
p-IC_6H_4O	3909.29072	3582.93745	326.35327
C_6H_5O	974.04614	646.97501	327.07113

Table S3. Summary of the observed DBS vibrational levels in the photodetachment spectra for *p*-$FC_6H_4O^-$, *p*-$ClC_6H_4O^-$, *p*-$BrC_6H_4O^-$, *p*-$IC_6H_4O^-$ in Figure 1. The corresponding wavelengths, photon energies, energy shifts with respect to peak 0 and assignments are given. The uncertainty is given by the number in the parentheses.

Peak	Wavelength (nm)	Photon Energy (cm^{-1})	Shift (cm^{-1})	Assignment
***p*-$FC_6H_4O^-$**				
0	**540.49**	**18502(3)**	**0**	**Ground DBS**
1	540.23	18511(3)	9	$0_0'$
2	531.45	18816(5)	314	$19'_1$
3	527.56	18955(5)	453	$11'_1/19'_120'_1$
4	526.35	18999(5)	497	$18'_1$
5	515.38	19403(5)	901	$11'_2/11'_119'_120'_1$
6	514.15	19450(5)	948	$11'_118'_1$
7	503.70	19853(5)	1351	$11'_3/11'_211'_120'_2$
8	502.63	19895(5)	1393	$11'_218'_1$
***p*-$ClC_6H_4O^-$**				
0	**497.85**	**20086(5)**	**0**	**Ground DBS**
1	488.59	20467(5)	381	$11'_1/19'_120'_1$
2	486.08	20573(5)	487	$11'_120'_1$
3	482.16	20740(5)	654	$10'_1$
***p*-$BrC_6H_4O^-$**				
0	**487.17**	**20527(5)**	**0**	**Ground DBS**
1	481.17	20783(5)	256	$19'_1$
2	480.27	20822(5)	295	$11'_1$
3	476.05	21006(5)	479	$18'_1$
4	473.67	21112(5)	585	$11'_2$
5	473.15	21135(5)	608	$10'_1$
***p*-$IC_6H_4O^-$**				
0	**476.36**	**20993(5)**	**0**	**Ground DBS**
1	470.87	21237(5)	244	$11'_1$
2	465.82	21468(5)	475	$18'_1$
3	463.47	21576(5)	583	$10'_1$
4	458.25	21822(5)	829	$10'_111'_1$

Table S4. Summary of the observed vibrational peaks from the resonant and non-resonant photoelectron spectra of *p*-$FC_6H_4O^-$. The energy shifts relative to peak 0_{00} are given. The uncertainty is given in the parentheses. The theoretical frequencies are from Table S8.

Peak	Binding Energy (eV)	Shift (cm^{-1})	Assignment	Theor. freq. (cm^{-1})
0_{00}	2.2950(6)	0	Neutral Ground State	
A	2.3328(7)	305	19^1	315
B	2.3505(8)	448	11^1	457
C	2.3565(7)	496	18^1	509
D	2.3891(10)	759	$11^1 19^1$	
E	2.4063(9)	898	11^2	
F	2.4123(7)	946	$11^1 18^1$	
G	2.4622(9)	1349	11^3	
H	2.4671(9)	1388	$11^2 18^1$	
a	2.3103(9)	123	20^1	132
b	2.3666(10)	577	$11^1 20^1$	
c	2.4222(7)	1026	$11^2 20^1$	
d	2.4445(7)	1206	$11^2 19^1$	
e	2.4505(7)	1254	$11^1 18^1 19^1$	

Table S5. Summary of the observed vibrational peaks from the resonant and non-resonant photoelectron spectra of *p*-$ClC_6H_4O^-$. The energy shifts relative to peak 0_{00} are given. The uncertainty is given in the parentheses. The theoretical frequencies are from Table S8.

Peak	Binding energy (eV)	Shift (cm^{-1})	Assignment	Theor. freq. (cm^{-1})
0_{00}	2.4917(8)	0	Neutral Ground State	
A	2.5386(7)	378	11^1	379
B	2.5520(8)	486	$11^1 20^1$	
C	2.5726(7)	652	10^1	650
a	2.5048(10)	106	20^1	108
b	2.5258(8)	275	19^1	274

Table S6. Summary of the observed vibrational peaks from the resonant and non-resonant photoelectron spectra of *p*-$BrC_6H_4O^-$. The energy shifts relative to peak 0_{00} are given. The uncertainty is given in the parentheses. The theoretical frequencies are from Table S8.

Peak	Binding energy (eV)	Shift (cm^{-1})	Assignment	Theor. freq. (cm^{-1})
0_{00}	2.5480(7)	0	Neutral Ground State	
A	2.5842(8)	292	11^1	291
B	2.6076(6)	481	18^1	487
C	2.6201(7)	582	11^2	
D	2.6230(9)	605	10^1	610
a	2.5597(6)	94	20^1	95
b	2.5957(6)	385	11^120^1	

Table S7. Summary of the observed vibrational peaks from the resonant and non-resonant photoelectron spectra of *p*-$IC_6H_4O^-$. The energy shifts relative to peak 0_{00} are given. The uncertainty is given in the parentheses. The theoretical frequencies are from Table S8.

Peak	Binding energy (eV)	Shift (cm^{-1})	Assignment	Theor. freq. (cm^{-1})
0_{00}	2.6094(5)	0	Neutral Ground State	
A	2.6400(7)	245	11^1	247
B	2.6701(8)	490	11^2	
C	2.6820(8)	585	10^1	593
D	2.6992(11)	724	11^3	

Table S8. The theoretical harmonic frequencies of the four neutral radicals, *p*-FC_6H_4O, *p*-ClC_6H_4O, *p*-BrC_6H_4O, and *p*-IC_6H_4O, calculated at the B3LYP/6-311++G(d,p) level of theory.

Mode	Symmetry	FC_6H_4O	ClC_6H_4O	BrC_6H_4O	IC_6H_4O
ν_1	A_1	3205	3204	3203	3204
ν_2		3189	3188	3187	3188
ν_3		1598	1579	1572	1571
ν_4		1492	1493	1493	1496
ν_5		1429	1419	1417	1424
ν_6		1252	1170	1170	1175
ν_7		1142	1080	1054	1043
ν_8		989	988	985	987
ν_9		816	806	804	806
ν_{10}		764	650	610	593
ν_{11}		457	379	291	247
ν_{12}	A_2	964	972	973	977
ν_{13}		777	784	784	794
ν_{14}		385	380	378	380
ν_{15}	B_1	950	959	957	983
ν_{16}		856	851	850	863
ν_{17}		710	704	685	714
ν_{18}		509	499	487	495
ν_{19}		315	274	262	257
ν_{20}		132	108	95	88
ν_{21}	B_2	3203	3202	3201	3202
ν_{22}		3190	3188	3188	3188
ν_{23}		1528	1501	1496	1493
ν_{24}		1438	1432	1428	1433
ν_{25}		1291	1287	1287	1290
ν_{26}		1267	1268	1268	1268
ν_{27}		1101	1110	1110	1113
ν_{28}		624	616	613	613
ν_{29}		461	455	453	452
ν_{30}		370	275	228	199